Atom Indonesia

Journal homepage: http://atomindonesia.brin.go.id

Evaluation of Radiological and Dosimetric Characteristics of 3D-Printed High-Impact Polystyrene for Radiotherapy Bolus

F. A. Rizaldi[1], D. J. D. H. Santjojo[1], L. A. Abrar[1], F. K. Hentihu[2], S. Herwiningsih[1*]

[1]*Physics Department, Faculty of Mathematics and Natural Sciences, Brawijaya University, Malang 65145, Indonesia*
[2]*Radiotherapy Department, Lavalette Hospital, Malang 65111, Indonesia*

ARTICLE INFO

Article history:
Received 3 October 2025
Received in revised form 10 February 2026
Accepted 4 March 2026

Keywords:
Post-Mastectomy Radiation Therapy (PMRT)
Electron beam radiation therapy
Linear accelerator
3D-Printed bolus
High-impact polystyrene
Tissue-mimicking material

ABSTRACT

Post-Mastectomy Radiation Therapy (PMRT) requires optimal dose delivery to the skin surface. However, the skin-sparing effect often leads to superficial underdosage. Although the use of a bolus can increase the surface dose, conventional boluses often have limitations in conforming to irregular surfaces, such as the breast. The Three-Dimensional (3D) printing with High-Impact Polystyrene (HIPS) offers a potential solution for fabricating patient-specific boluses based on Computed Tomography (CT) images. This study aims to evaluate the radiological and dosimetric characteristics of 3D-printed HIPS boluses at different thicknesses and infill densities, and to investigate the conformity of breast-shaped 3D-printed HIPS boluses on mannequin breasts. Plate-shaped 3D-printed HIPS boluses with thicknesses of 6, 8, and 10 mm at 20%, 40%, 60%, and 80% infill densities, as well as breast-shaped boluses with a thickness of 6 mm at 20%, 40%, 60%, and 80% infill densities, were fabricated using a 3D printer with HIPS filament. The material characterizations encompassed Hounsfield Unit (HU), Relative Electron Density (RED), Percentage Surface Dose (PSD), Stopping Power (SP), and Continuous Slowing Down Approximation (CSDA) range. The results indicated HU values of −539 to −248 and RED of 0.56 to 0.75. Surface dose assessment indicated PSD levels of 92% to 97% of the prescribed dose. The total stopping power was observed to vary from 0.143 to 0.167 MeV/mm, while the corresponding CSDA range decreased from 42.8 to 36.7 mm. Increasing infill density resulted in higher HU, RED, and PSD values, and improved bolus homogeneity, but reduced CSDA value. The optimal configuration was identified as an 8 mm thickness at 80% infill density. The breast-shaped boluses on mannequin breast exhibited the air gap volumes ranging from 1.14 to 1.86 cm^3. The 3D-printed HIPS boluses show potential to be integrated into the existing clinical workflow.

INTRODUCTION

Post-Mastectomy Radiation Therapy (PMRT) is a radiation therapy delivered after the surgical removal of the entire breast with a malignant tumour (mastectomy) to eradicate any residual cancer cells. This approach has shown promising results in reducing the local recurrence rate and improving the patient's survival rate [1]. Mastectomy causes the target volume of treatment to be shifted closer to the skin surface [2,3]. However, delivering an optimal radiation dose to the skin surface is challenging due to the skin-sparing effect, which often results in superficial underdosage [4-6].

The International Commission on Radiation Units and Measurements (ICRU) Report 71 recommends that the PTV should receive 95% - 100% of the prescribed dose [7]. The Percentage Surface Dose (PSD) has been reported to reach 70.8% of the prescribed dose for a 6 MeV electron beam with a field size of $10 \times 10\ cm^2$, produced by a Varian 2300 C/D linear accelerator [8]. This surface dose can be increased by using a bolus during radiotherapy [9].

Boluses are tissue-equivalent materials used to increase the surface dose by shifting 95% - 100% of the Percentage Depth Dose (PDD) closer to the

*Corresponding author.
E-mail address: herwin@ub.ac.id
DOI: https://doi.org/10.55981/aij.2026.1813

skin surface [10]. A previous study recommended High-Impact Polystyrene (HIPS) as a bolus material due to the resemblance between the PDD distribution of an electron beam within HIPS and that of a tissue-equivalent material [11]. Previous studies also reported that the HIPS filament exhibited both physical and radiological characteristics similar to those of adipose tissue [12,13].

A recent study has shown that three-dimensional (3D) printing technology enables the fabrication of patient-specific boluses based on Computed Tomography (CT) images [14]. This advancement improves the bolus conformity to the irregular skin surfaces, thereby minimizing the air gaps between the bolus and the skin surface [15]. The 3D-printed boluses are commonly printed at 100% infill density to minimize the internal pore sizes [15,16]. Although using infill densities below 100% reduces printing duration and filament consumption, it increases the internal pore size, which compromises the bolus characteristics [13,17,18]. A recent study has shown that the gyroid infill pattern yields smaller internal pore sizes compared to the grid, rectilinear, and cubic infill patterns at the same infill densities ranging from 40% to 60% [19].

This study presents a novel optimization of 3D-printed HIPS bolus thickness and infill density by utilizing the gyroid infill pattern. This optimized configuration is designed to minimize the printing duration and filament consumption while maintaining acceptable radiological and dosimetric characteristics. Therefore, this study aims to evaluate the radiological and dosimetric characteristics of 3D-printed HIPS at different thicknesses and infill densities for radiotherapy bolus. The radiological characteristics evaluated are the Hounsfield Unit (HU) and Relative Electron Density (RED), while the dosimetric characteristics evaluated are the PSD, Stopping Power (SP), and Continuous Slowing Down Approximation (CSDA). Furthermore, this study investigates the conformity of breast-shaped 3D-printed HIPS boluses on mannequin breasts.

METHODS

Fabrication of plate-shaped 3D-printed HIPS boluses

Plate-shaped HIPS boluses with a surface area of 120 mm × 120 mm and thicknesses of 6 mm, 8 mm, and 10 mm were designed using Blender software version 4.3.1 (Blender Foundation, Amsterdam, Netherlands). The bolus thicknesses were determined based on the depth of 95% of the prescribed dose for a 6 MeV electron beam in a water phantom, which was 8 mm. The plate-shaped HIPS bolus designs were sliced using CreatWare software version 7.2.0 (CreatBot, Zhengzhou, China) with gyroid infill densities of 20%, 40%, 60%, and 80%, and subsequently fabricated using an Inova3D i4030 3D printer (PT Proinnov Teknologi Indonesia, Tangerang, Indonesia). The printing parameters used to fabricate the plate-shaped 3D-printed HIPS boluses are summarized in Table 1.

The printing parameters in Table 1 were determined through iterative trials of printing tests using HIPS filament (Indofilam, Bandung, Indonesia) on an Inova3D i4030 3D printer to achieve high print quality while maintaining a short printing duration. Post-processing was performed to smooth the sharp edges of the plate-shaped 3D-printed HIPS boluses using sandpaper. Figure 1 shows the gyroid infill pattern at different infill densities simulated using CreatWare software.

Table 1. The printing parameters used to fabricate the plate-shaped and breast-shaped 3D-printed HIPS boluses.

Printing parameter	3D-printed HIPS bolus	
	Plate-shaped	Breast-shaped
Nozzle temperature	240 °C	240 °C
Chamber temperature	65 °C	65 °C
Bed temperature	110 °C	110 °C
Perimeter wall	2	2
Top and bottom solid layers	5	5
Fill angle	45°	45°
Support materials	-	Organic
Nozzle diameter	0.4 mm	0.2 mm
Maximum nozzle diameter	0.8 mm	0.4 mm
Layer height	0.4 mm	0.2 mm
Inner perimeter speed	40 mm/s	12 mm/s
Infill speed	40 mm/s	35 mm/s
External perimeter speed	26 mm/s	12 mm/s
Support materials speed	-	35 mm/s

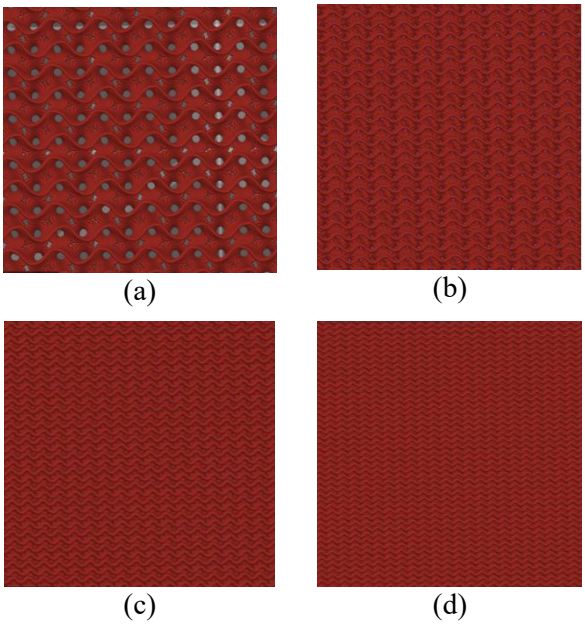

Fig. 1. Gyroid infill pattern at infill densities of (a) 20%, (b) 40%, (c) 60%, and (d) 80%.

In this study, gyroid infill densities above 80% were excluded because they caused extreme vibrations on the 3D printer, compromising the printing stability and leading to poor dimensional accuracy of the printed object. Conversely, gyroid infill densities below 20% were excluded due to the formation of large overhanging structures, causing the top layer to collapse onto the bottom layer.

Fabrication of breast-shaped 3D-printed HIPS boluses

The female mannequin was scanned using a SOMATOM go.Sim Computed Tomography (CT) simulator (Siemens Healthineers, Erlangen, Germany) with a tube voltage of 120 kVp and a tube current of 44 mAs. The CT image of the female mannequin was converted into the stereolithography (STL) format using Fiji software version 1.8.0_322 (The National Institutes of Health, Maryland, United States). The surface mesh of the female mannequin was smoothed using MeshLab software version 2023.12 (ISTI-CNR Research Center, Pisa, Italy) by applying the Taubin filter ($\mu = -0.53, \lambda = 0.5,$ and a smoothing step of 20). The Taubin filter was selected due to its ability to smooth curves and surfaces without shrinkage [20].

The breast-shaped HIPS bolus was designed using Blender software by isolating the breast mesh geometry from the female mannequin. Subsequently, a lattice modifier was applied to a 6 mm thick plate-shaped HIPS design, followed by a shrinkwrap modifier to conform the design to the surface mesh of the mannequin breast. The breast-shaped HIPS bolus design was sliced using CreatWare software with gyroid infill densities of 20%, 40%, 60%, and 80%, and subsequently fabricated using an Inova3D i4030 3D printer. The printing parameters used to fabricate the breast-shaped 3D-printed HIPS boluses are summarized in Table 1. Post-processing was performed to remove the support materials from the breast-shaped 3D-printed HIPS boluses.

CT number measurements

All plate-shaped 3D-printed HIPS boluses were scanned using a SOMATOM go.Sim CT simulator with a tube voltage of 120 kVp and a tube current of 44 mAs [21]. The CT numbers in HU were measured using MicroDicom software version 2025.1 (MicroDicom Ltd, Sofia, Bulgaria) at 27 Regions of Interest (ROIs). These ROIs were evenly distributed among the top layer, infill layer, and bottom layer, as shown in Fig. 2.

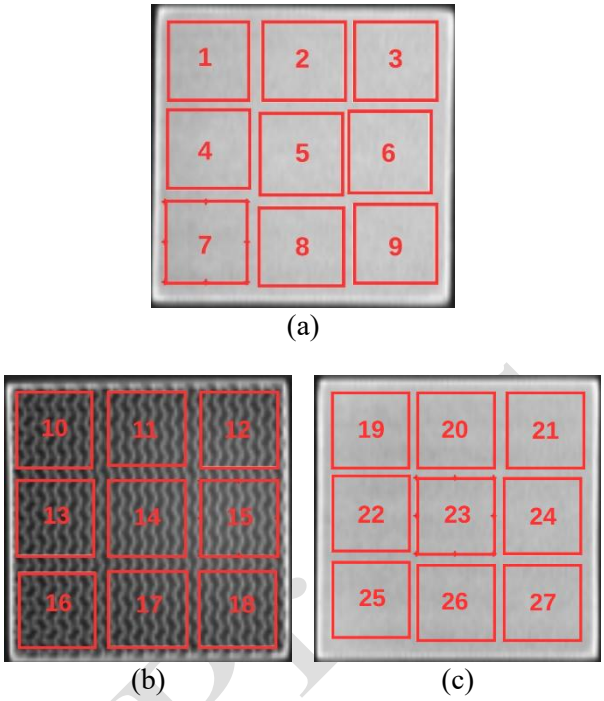

Fig. 2. CT number measurement at the (a) top layer, (b) infill layer, and (c) bottom layer.

The mean CT number was determined by averaging the CT number measurements across 27 ROIs, while the measurement uncertainty was expressed as the standard deviation.

RED and ED calculations

The RED of each plate-shaped 3D-printed HIPS bolus was calculated using Eq. (1) or Eq. (2), depending on its corresponding CT number [21]:

$$RED = 1.052 + 0.00048N_{CT>100HU} \quad (1)$$

$$RED = 1.000 + 0.001N_{CT<100HU} \quad (2)$$

Where RED is the relative electron density, $N_{CT>100}$ and $N_{CT<100}$ denote the CT number above and below 100 HU, respectively [21]. The electron density of each plate-shaped 3D-printed HIPS bolus was calculated using Eq. (3) [22].

$$\rho_e = RED * \rho_{e,w} \quad (3)$$

Where ρ_e is the electron density $(electrons/mm^3)$ and $\rho_{e,w}$ is the electron density of water $(electrons/mm^3)$ [22]. The electron density of water used is $3.34 \times 10^{-20}\ electrons/mm^3$ [23]. The propagation of uncertainty for both RED and ED values was derived from the standard deviation of the CT number measurements.

PSD measurement

The absorbed dose measurements were conducted using an advanced Markus plane-parallel electron chamber TM34045 (PTW, Freiburg, Germany) and RW3 slab phantom (PTW, Freiburg, Germany), following the International Atomic Energy Agency (IAEA) Technical Reports Series No. 398 (TRS-398) protocols [24]. The PSD measurements were performed using a 6 MeV electron beam produced by an Elekta Synergy linear accelerator (Elekta, Stockholm, Sweden), with a Source-to-Surface Distance (SSD) of 100 cm, an applicator of 10×10 cm^2, and a field size of 10×10 cm^2 [21,24]. The slab phantom surface was defined as the PTV region. No chamber positioning tolerance or effective point of measurement correction was applied during the measurements. The PSD measurement setup is shown in Fig. 3.

The absorbed dose on the slab phantom surface was measured with and without the plate-shaped 3D-printed HIPS bolus, while the absorbed dose at the depth of maximum dose was measured without the bolus. The PSD was calculated using Eq. (4) [9].

$$PSD = \frac{D_s}{D_{max}} \times 100\% \quad (4)$$

Where PSD is the percentage surface dose (%), D_s is the absorbed dose on the slab phantom surface, and D_{max} is the absorbed dose at the depth of maximum dose [9].

Fig. 3. PSD measurements setup.

SP and CSDA calculations

The SP and CSDA of a 6 MeV electron beam in a plate-shaped 3D-printed HIPS bolus at different infill densities were calculated using the National Institute of Standards and Technology (NIST) database using the Electron Stopping-Power and Range Tables (ESTAR) program (National Institute of Standards and Technology, Gaithersburg, USA) [25]. mass fraction percentages of polystyrene, polybutadiene, and air within the bolus.

The bulk densities of the HIPS filament and the 3D-printed boluses at different infill densities were calculated by dividing their mass by their bulk volume [26]. The polystyrene and polybutadiene content within the HIPS filament was analyzed using Fourier Transform Infrared Spectroscopy (FTIR). The concentrations of these contents were calculated by applying the Beer-Lambert Law to the aromatic and non-aromatic C=C bond peaks, respectively [27], utilizing the molar absorption coefficients reported in [28]. The mass fraction percentages of polystyrene and polybutadiene within the HIPS filament were derived from their concentration values.

The mass fraction percentages of the HIPS filament and air within the 3D-printed boluses were calculated based on the volume fraction percentages derived from the corresponding infill density [13]. The mass fraction percentage of the HIPS filament was expanded into the mass fraction percentages of polystyrene and polybutadiene. The air composition and corresponding mass fraction percentages from the standard atmospheric composition reported in [29] and the air density reported in [30] were used in this study. These values were input into the ESTAR program to compute the SP and CSDA of the bolus. The SP and CSDA for adipose tissue were calculated following the same procedure used for the boluses. The atomic composition of the adipose tissue reported in [31] was used in this study.

Air gap volume measurements

The breast-shaped 3D-printed HIPS bolus was positioned on the mannequin breast and scanned using a SOMATOM go.Sim CT simulator with a tube voltage of 120 kVp, a tube current of 44 mAs, and a slice thickness of 2 mm. The air gap area between the bolus and the mannequin breast across all slices of the CT image was measured using Fiji software. The total air gap volume was calculated by multiplying the air gap area by the slice thickness for each slice, and then summing these values across the entire slice of the CT image.

RESULTS AND DISCUSSION

The CT images of the infill layer within the plate-shaped 3D-printed HIPS boluses are presented in Fig. 4.

Figure 4 shows that the boluses at infill densities of 20% and 40% exhibited a heterogeneous appearance composed of dark and bright pixels, where the dark pixels represent internal pores and the bright pixels represent the HIPS material. Conversely, the boluses at infill densities of 60% and 80% exhibited a homogeneous appearance composed of uniformly bright pixels. However, this homogeneous appearance does not imply the absence of internal pores, but rather indicates that the internal pore sizes were smaller than the CT simulator spatial resolution of 1 mm. Consequently, each pixel in the CT image contained a mixture of both HIPS material and air, which resulted in a mean HU value. Since a higher infill density increases the volume fraction of HIPS material relative to air, the CT images of the bolus appear brighter as the infill density increases. This result aligns with a previous study that reported the presence of internal pores with sizes of less than 1 mm within the infill layer of 3D-printed HIPS with gyroid infill densities of 60% and 80%, as observed using a digital microscope [13]. The HU, ED, and RED values of plate-shaped 3D-printed HIPS boluses are summarized in Table 2.

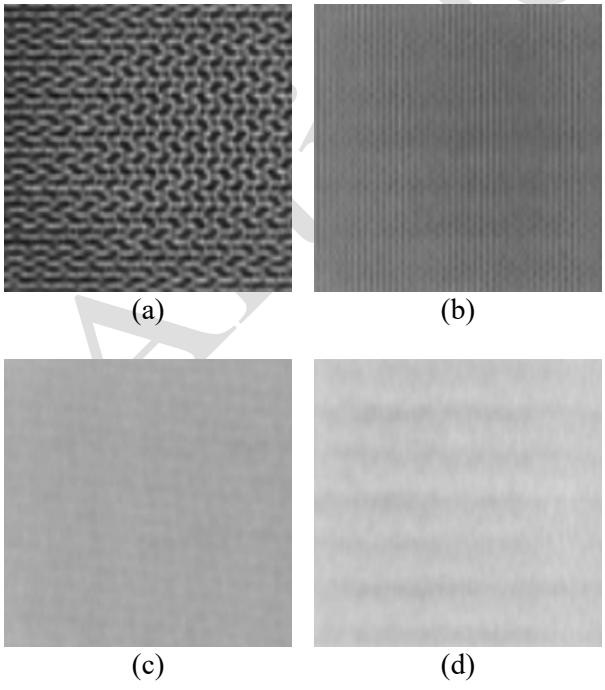

Fig. 4. CT images of infill layer within the plate-shaped 3D-printed HIPS boluses at infil densities of (a) 20%, (b) 40%, (c) 60%, and (d) 80%.

Table 2. HU, ED, and RED of plate-shaped 3D-printed HIPS boluses at different thicknesses and infill densities.

Thickness (mm)	ID[a] (%)	HU	ED (10^{20} electrons/ mm^3)	RED
6	20	-423 ± 193	1.93 ± 0.65	0.58 ± 0.19
	40	-392 ± 167	2.03 ± 0.57	0.61 ± 0.17
	60	-348 ± 176	2.18 ± 0.59	0.65 ± 0.18
	80	-248 ± 93.9	2.51 ± 0.31	0.75 ± 0.09
8	20	-439 ± 265	1.87 ± 0.88	0.56 ± 0.26
	40	-394 ± 214	2.02 ± 0.71	0.61 ± 0.21
	60	-348 ± 152	2.18 ± 0.51	0.65 ± 0.15
	80	-263 ± 90.4	2.46 ± 0.30	0.74 ± 0.09
10	20	-426 ± 267	1.92 ± 0.65	0.58 ± 0.19
	40	-383 ± 201	2.06 ± 0.67	0.62 ± 0.20
	60	-334 ± 149	2.22 ± 0.51	0.67 ± 0.15
	80	-255 ± 101	2.48 ± 0.34	0.74 ± 0.10

[a] Infill Density (ID)

These HU values were obtained directly from CT images reconstructed using the Q40 kernel and Sinogram-Affirmed Iterative Reconstruction (SAFIRE), without any additional post-processing or external filtering. Table 2 shows that the 3D-printed HIPS boluses exhibited negative HU values and RED values of less than one. These results indicate that the 3D-printed HIPS boluses are less dense than water. In addition, Table 2 demonstrates that higher infill densities increased the HU, ED, and RED values, resulting in a whiter appearance on the CT images of the bolus, as presented in Fig. 4. This phenomenon arises because a higher infill density results in increased HIPS filament deposition within the bolus, which corresponds to a greater number of bound electrons present within the bolus [32]. The ED and RED values of the 3D-printed HIPS boluses in Table 2 align with those reported in [13], even though the methods used for calculating RED were different.

Table 2 shows that the HU values of the bolus exhibited significant standard deviations, which increased as the infill density decreased. This is attributed to the entrapped air within the internal pores of the infill layers. Due to the substantial contrast between the HU values of HIPS and air, the distribution of HU values became less uniform and exhibited greater variation, particularly at lower infill densities where the internal pore sizes were larger.

The RED values of tissue-mimicking reference materials for adipose tissue and lung tissue were 0.93 and 0.43, respectively [33]. Among the tested samples, the 3D-printed HIPS bolus at 80% infill density exhibited RED values closest to the tissue-mimicking reference material for adipose tissue. Nevertheless, its RED value remained lower than that of the tissue-mimicking reference material for adipose tissue. In contrast, the 3D-printed HIPS bolus at 20% infill density was closest to the tissue-mimicking reference material for lung tissue. This result reflects the internal structure of the bolus.

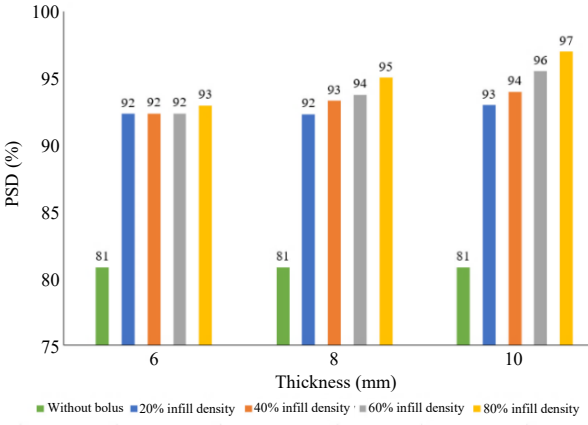

Fig. 5. The PSD of a 6 MeV electron beam on a slab phantom surface with and without the plate-shaped 3D-printed HIPS bolus.

Table 3. Total SP and CSDA of a 6 MeV electron beam within the 3D-printed HIPS boluses and their relative difference compared to those of adipose tissue.

ID[a] (%)	Total SP (MeV/mm)		Relative difference (%)
	3D-printed HIPS bolus	Adipose tissue	
20	0.143	0.186	23.2
40	0.152		18.3
60	0.158		14.9
80	0.167		10.5
ID[a] (%)	**CSDA (mm)**		**Relative difference (%)**
	3D-printed HIPS bolus	**Adipose tissue**	
20	42.8	32.8	30.6
40	40.2		22.7
60	38.6		17.7
80	36.7		12.0

[a] Infill Density (ID)

At 20% infill density, the presence of internal pores mimics the alveolar structure of lung tissue. As the heterogeneous structure of lung tissue enhances the lateral scattering effects of the electron beam [32,34], the 3D-printed HIPS at 20% infill density may be more suitable for use as a lung phantom rather than as a bolus. Figure 5 shows the PSD of a 6 MeV electron beam on a slab phantom surface with and without the plate-shaped 3D-printed HIPS bolus.

The increase in PSD with higher infill density is attributed to the higher ED within the bolus. The greater number of bound electrons within the bolus, indicated by a higher ED, increases the probability of Coulomb force interactions between the electron beam and the bolus materials [32]. This increases the number of charged particles reaching the bolus-phantom interface, thereby increasing the PSD. A higher infill density also minimizes air perturbation within the bolus, as it results in smaller pore sizes. The presence of air cavities within the internal pores enhances the lateral scattering effects of the electron beam [32,34]. This reduces the number of charged particles reaching the bolus-phantom interface, thereby decreasing the PSD.

The bolus thickness determines the electron beam trajectory length within the bolus. A longer electron path increases the probability of Coulomb force interactions between the electron beam and the bolus material [32]. This increases the number of charged particles reaching the bolus-phantom interface, causing an increase in the PSD. These findings are consistent with previous studies that reported similar effects of bolus thickness [35] and infill density [36] on PSD, despite the use of different bolus materials and infill patterns.

Figure 5 shows that at lower infill densities, increasing the bolus thickness has a less significant impact on increasing PSD. This is evident in the plate-shaped 3D-printed HIPS boluses at 20% infill density, which showed minimal variation in PSD across different thicknesses. This occurs because lower infill densities result in a larger internal pore volume, which reduces the effective material thickness encountered by the electron beam. This is because increasing the bolus thickness also increases the number of internal pores [13]. Consequently, the added physical thickness is compensated for by the increasing number of internal pores within the bolus. As a result, the effective material thickness exhibits minimal variation despite the increase in physical thickness.

Given that the slab phantom surface was defined as the PTV region, Fig. 5 shows that the PSD of a 6 MeV electron beam without a bolus was 81%, which failed to meet the PTV dose range recommended by ICRU Report 71. However, the use of a bolus with configurations of 10 mm thickness at 60% infill density, and both the 8 mm and 10 mm thicknesses at 80% infill density, each increased the PSD to at least 95%, which met the PTV dose range recommended by ICRU Report 71. Table 3 shows the total SP and CSDA of a 6 MeV electron beam within the plate-shaped 3D-printed HIPS boluses.

As infill density increases, the total SP increases, which in turn decreases the CSDA. This occurs because the higher ED at increased infill percentages raises the probability of Coulomb force interactions between incident electrons and the bolus material. As a result, the amount of electron beam energy lost per unit thickness increases, causing the energy to be depleted faster, thereby reducing the average penetration depth [32]. Consistent with these principles, the plate-shaped 3D-printed HIPS bolus at 80% infill density exhibited the smallest relative differences for both total SP and CSDA compared to those of adipose tissue. This aligns

with the radiological characterization results, which demonstrated that the bolus at 80% infill density most closely mimicked adipose tissue compared to other infill densities.

The radiological and dosimetric characteristics of the 3D-printed HIPS boluses were evaluated comprehensively, as both characteristics must be satisfied simultaneously. Specifically, the three configurations that achieved a PSD of at least 95% of the prescribed dose were the 10 mm thickness at 60% infill density, and both the 8 mm and 10 mm thicknesses at 80% infill density. The 80% infill density is preferred over the 60% density because its homogeneity, RED, SP, and CSDA values more closely mimic adipose tissue. Additionally, as shown in Table 4, at the same infill density, the bolus with a thickness of 8 mm requires a shorter printing duration and consumes less HIPS filament compared to the bolus with a thickness of 10 mm.

Therefore, the bolus with an 8 mm thickness at 80% infill density is considered the optimal configuration. Figure 6 shows the CT images of the breast-shaped 3D-printed HIPS boluses placed on the mannequin breasts.

Figure 6 shows that air gaps were still present between the bolus and the mannequin breast, even though the bolus was fabricated based on CT images of the mannequin breast itself. This likely occurred due to the lack of transparency of the bolus material, which made it difficult to position the bolus accurately on the mannequin breast surface. Despite the limitations regarding the bolus material opacity, the observed air gap volumes presented in Table 5 are consistent with those reported in previous studies on nose-shaped 3D-printed Thermoplastic Polyurethane (TPU) and Polylactic Acid (PLA) boluses [19], and pelvic-shaped 3D-printed Polyethylene Terephthalate Glycol (PETG) bolus [37].

Table 4. Total HIPS filament consumption and printing duration for fabricating the plate-shaped 3D-printed HIPS boluses at different thicknesses and infill densities.

Thickness (mm)	Infill density (%)	HIPS filament consumption (gram)	Printing duration (minutes)
6	20	64.4	108
	40	69.4	119
	60	73.6	130
	80	78.4	142
8	20	70.7	119
	40	80.5	142
	60	89.2	164
	80	99.4	191
10	20	77.1	131
	40	91.7	165
	60	105.4	199
	80	119.9	241

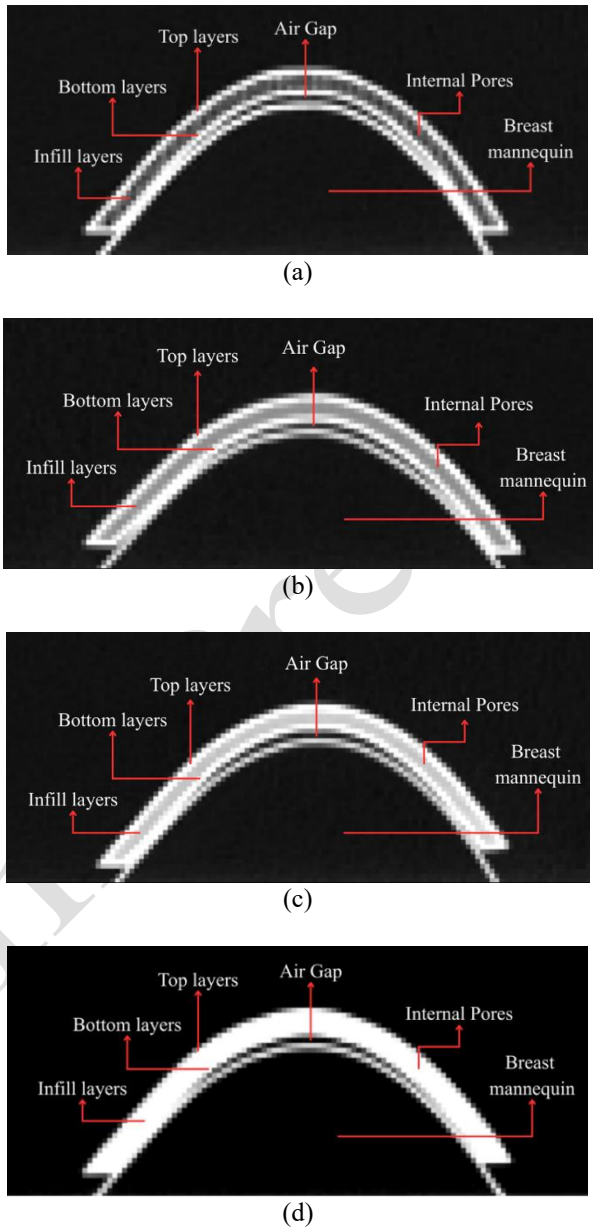

Fig. 6. CT image of the breast-shaped 3D-printed HIPS boluses at infill densities of (a) 20%, (b) 40%, (c) 60%, and (d) 80% placed on the mannequin breasts.

Table 5. Air gap volumes between the mannequin breast surface and the breast-shaped 3D-printed HIPS bolus at different infill densities.

Infill density (%)	Air gap volume (cm^3)
20	1.14
40	1.49
60	1.86
80	1.63

As presented in Table 5, the air gap volume became larger as the infill density increased up to 60%, but subsequently decreased at 80%. Theoretically, altering the infill density changes the amount of filament deposited within the infill layers while the external geometric volume remains constant [13]. Consequently, this should not impact

the bolus conformity, and the air gap volumes should theoretically not be influenced by the infill density. Therefore, the observed variations in air gap volumes are likely attributed to positioning inconsistencies caused by the lack of transparency of the bolus material, which made it difficult to ensure precise positioning for each bolus on the breast mannequin.

There are several limitations in this study that should be noted. The HU values are inherently dependent on the specific CT simulator parameter settings [38] and the reconstruction kernel used [39]. Consequently, these quantitative values may exhibit slight variations across different CT simulators. The physical characteristics of the bolus are subject to variability based on the printing parameters used [13]. This study maintained the constant printing parameters as detailed in Table 1. Additionally, the dosimetric characterization was limited to the use of planar bolus geometry under a 6 MeV electron beam. The air gap measurements utilized the mannequin breasts, which represent simplified breast geometry and possess rigid surfaces. This differs significantly from the deformable nature of breast tissue.

To address these limitations, further studies are required to evaluate bolus performance across a wider range of printing parameters and beam energies, while exploring transparent filaments to address positioning challenges. It is also recommended to verify HU consistency across various CT simulators and to validate air gap measurements through clinical implementation to account for the deformable nature of breast tissue. Despite these limitations, the study demonstrates that the 3D-printed HIPS bolus holds significant potential for radiotherapy applications and could integrate well into the existing clinical workflow, as shown in Fig 7.

The proposed clinical workflow begins by utilizing the patient's diagnostic CT images. These images are processed to extract the external body contour, which serves as the template for designing the breast-shaped 3D-printed HIPS bolus. Once fabricated, the bolus is positioned on the patient's breast surface during the CT simulation procedure to capture the actual setup and electron density information. Subsequently, a treatment plan is generated based on this setup. Prior to the final treatment delivery, a Patient-Specific Quality Assurance (PSQA) is conducted to verify the dose distribution and ensure concordance between the calculated and measured doses. Finally, upon successful verification, the radiation treatment is delivered to the patient.

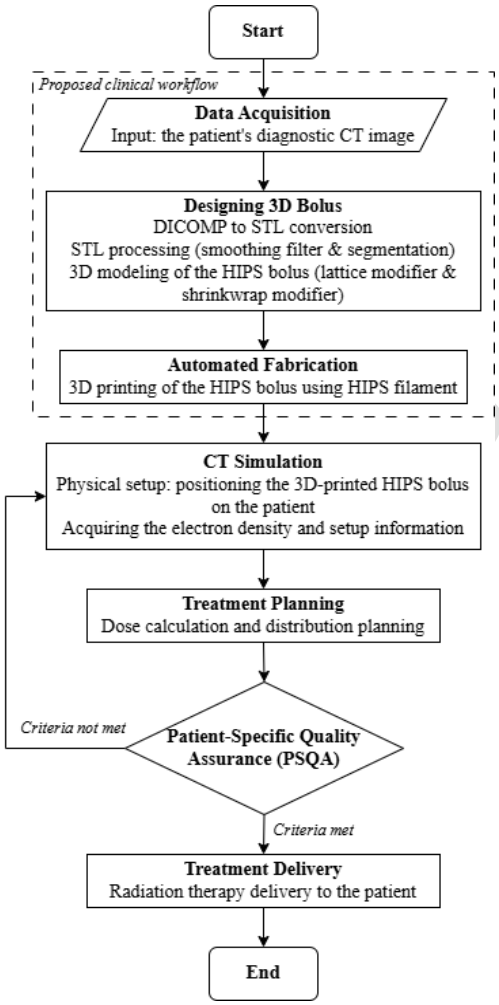

Fig. 7. Proposed clinical workflow with the 3D-printed HIPS bolus.

The proposed clinical workflow shows many similarities with the existing clinical workflow using conventional boluses. When a commercial sheet bolus is unavailable, the existing workflow relies on a manually fabricated bolus made of plasticine, playdoh, natural rubber, or paraffin wax [9]. The primary distinction lies in the fabrication process, where the 3D-printing method utilizes the CT image for designing the 3D bolus, followed by automated fabrication using a 3D printer.

This shift from manual to automated fabrication process reduces the physical workload for medical physicists. The current process of designing the 3D bolus requires time for DICOM to STL conversion, smoothing filtering, segmentation, and 3D modeling. However, this proposed clinical workflow demonstrates potential for future integration with Artificial Intelligence (AI) to automate the 3D bolus design process [40]. Thus, the integration of 3D-printed boluses requires minimal adaptation to the existing clinical workflow while offering improved bolus conformity for irregular geometries.

CONCLUSION

This study demonstrated that increasing the gyroid infill density resulted in higher HU, ED, RED, PSD, and SP values, along with a reduced CSDA, and improved bolus homogeneity. Consequently, the higher infill densities improved both the radiological and dosimetric characteristics of the 3D-printed HIPS boluses, thereby enabling them to closely mimic the characteristics of adipose tissue. Among the tested samples, the plate-shaped 3D-printed HIPS bolus with a thickness of 8 mm at 80% infill density was identified as the optimal configuration. Furthermore, the breast-shaped HIPS boluses exhibited acceptable conformity with minimal air gap volumes between the bolus and the mannequin breast surface.

ACKNOWLEDGMENT

The author would like to thank Lavalette Hospital for providing the author with the opportunity to conduct research.

AUTHOR CONTRIBUTION

F. A. Rizaldi, S. Herwiningsih, and D. J. D. H. Santjojo equally contributed as the main contributors of this paper. All authors read and approved the final version of the paper

REFERENCES

1. K. Kim, J. Jung, H. Kim *et al*., Cancer Res. Treat. **54** (2022) 497.
2. F. K. Hentihu, A. K. Anto, R. S. Nugroho, Atom Indones. **48** (2022) 9.
3. S. Herwiningsih, A. Naba, S. Rianto *et al.*, Indo. Phy. Rev. **6** (2023) 284.
4. G. Wong, E. Lam, S. Bosnic *et al*., J. Med. Imaging Radiat. Sci. **51** (2020) 462.
5. N. H. Jannah, A. P. Hariyanto, S. Aisyah *et al*., *Surface Dose Analysis of Breast Cancer Post-Mastectomy with and Without Bolus Using the Three-Dimensional Conformal Radiotherapy Technique,* in: AIP Conf. Proc. (2023) 030008.
6. D. Lobo, C. Srinivas, S. Banerjee *et al*., Radiat. Environ. Biophys. **64** (2025) 77.
7. International Commission on Radiation Units and Measurements (ICRU), Prescribing, Recording, and Reporting Electron Beam Therapy (ICRU Report 71), ICRU, Bethesda, 2004.
8. B. J. Gerbi, J. A. Antolak, F. C. Deibel *et al*., Recommendations for Clinical Electron Beam Dosimetry: Supplement to the Recommendations of Task Group 25, John Wiley and Sons Ltd, Alexandria, 2009.
9. E. Endarko, S. Aisyah, C.C.C. Carina *et al*., J. Biomed. Phys. Eng. **11** (2021) 735.
10. F. Li, W. Hu, H. Li *et al*., Technol. Cancer Res. Treat. **24** (2025) 1.
11. I. Miloichikova, A. Bulavskaya, Y. Cherepennikov *et al*, Phy. Med. **64** (2019) 188.
12. X. Ma, M. Figl, E. Unger *et al*., Sci. Rep. **12** (2022) 14580.
13. F. A. Rizaldi, S. Herwiningsih, D. J. D. H. Santjojo *et al*., Indones. Phy. Rev. **9** (2026) 94.
14. P. Gong, G. Dai, X. Wu *et al.*, Breast **66** (2022) 317.
15. C. Zhang, W. Lewin, A. Cullen *et al*., Radiol. Phys. Technol. **16** (2023) 414.
16. Y. Zhang, Y. Huang, S. Ding *et al*, Cancer Med. **11** (2022) 1037.
17. E. Dąbrowska-Szewczyk, A. Zawadzka, P. Kowalczyk *et al*., Phy. Medica **110** (2023) 102600.
18. L. A. Abrar, S. Herwiningsih, J. A. E. Noor *et al*., Indones. Phy. Rev. **9** (2026) 49.
19. S. G. Gugliandolo, S. P. Pillai, S. Rajendran *et al*., Radiol. Phys. Technol. **17** (2024) 347.
20. G. Taubin, *A Signal Processing Approach to Fair Surface Design*, in: Seminal Graphics Papers: Pushing the Boundaries, Vol. 2, Association for Computing Machinery (ACM), New York (2023) 103.
21. A. Yuliandari, S. Oktamuliani, Harmadi *et al*., Iran. J. Med. Phy. **21** (2024) 211.
22. M. Bento, H. Cook, V. M. Anaya *et al*., Biomed. Phys. Eng. Express **10** (2024) 065005.
23. M. G. Herman, J. M. Balter, D. A. Jaffray *et al*., Med. Phys. **5** (2001) 712.
24. International Atomic Energy Agency (IAEA), Absorbed Dose Determination in External Beam Radiotherapy, An International Code of Practice for Dosimetry Based on Standards of Absorbed Dose to Water (Technical Reports Series No. 398), IAEA, Vienna, 2000.
25. I. F. Hussein, R. O. Abdaljalil, S. A. Mohammed *et al*., Kuwait J. Sci. **50** (2023) 545.
26. M. Boopathi, D. Khanna, P. Venkatraman *et al*., Asian Pac J Cancer Prev. **24** (2023) 141.

27. N. S. Giakoumakis, C. Vos, K. Janssens *et al*., Green Chem. **26** (2023) 340.

28. R. R. Hampton, Anal. Chem. **21** (1949) 923.

29. O. Rusoke-Dierich, Diving Medicine, Springer, Cham (2018) 41.

30. H. Suzuki, Y. Hasegawa, O. O. D. Afolabi *et al*., *Attempt to Quantify the Impact of Seasonal Air Density Variation on Operating Tip-Speed Ratio of Small Wind Turbines*, in: J. Phys. Conf. Ser., IOP Publishing, **2090** (2021) 012144.

31. Pacific Northwest National Laboratory (PNNL), Compendium of Material Composition Data for Radiation Transport Modeling, PNNL, Washington, 2021.

32. F. M. Khan, *Radiation Dosimetry*, in: The Physics of Radiation Therapy, 3rd ed., Lippincott Williams & Wilkins, Philadelphia (2003) 297.

33. S. Ohira, J. Mochizuki, T. Niwa *et al*., Radiol. Phys. Technol. **17** (2024) 458.

34. M. Kong and L. Holloway, Australas. Phys. Eng. Sci. Med. **30** (2007) 111.

35. K. H. Jung, D. H. Han, K. Y. Lee *et al*., App. Radiat. Isot. **209** (2024) 1.

36. R. Ricotti, D. Ciardo, F. Pansini *et al*., Phy. Med. 39 (2017) 25.

37. K. M. Wang, A. J. Rickards, T. Bingham *et al*., J. Appl. Clin. Med. Phys. **23** (2022) 1.

38. E. Setiawati, C. Anam, W. Widyasari *et al*., Atom Indones. **49** (2023) 61.

39. D. K. Jeong, S. S. Lee, J. E. Kim *et al*., Imaging Sci. Dent. **49** (2019) 273.

40. L. Ma, S. Yu, X. Xu *et al*., Mater. Today Bio **23** (2023) 100792.